Results in Engineering 19 (2023) 101312

Contents lists available at ScienceDirect

Results in Engineering

journal homepage: www.sciencedirect.com/journal/results-in-engineering

Effect of compressibility on industrial DC electric arcs

Mohamad Al-Nasser [a], Hadi Barati [b], Christian Redl [c], Anton Ishmurzin [d], Nikolaus Voller [d], Gernot Hackl [d], Manuel Leuchtenmüller [e], Menghuai Wu [f], Abdellah Kharicha [a,*]

[a] Christian Doppler Laboratory for Metallurgical Applications of Magnetohydrodynamics, Franz-Josef Street 18, 8700, Leoben, Austria
[b] K1-MET, Franz-Josef Street 18, 8700, Leoben, Austria
[c] INTECO Melting and Casting Technologies GmbH, Wienerstrasse 25, 8600, Bruck a.d. Mur, Austria
[d] RHI Magnesita, Department of Modelling and Simulation, Magnesitstrasse 2, 8700, Leoben, Austria
[e] Nonferrous Metallurgy, Erzherzog-Johann-Straße 3/II, 8700, Leoben, Austria
[f] Modeling and Simulation of Metallurgical Processes, Department of Metallurgy, Montanuniversität, Franz-Josef Street 18, 8700, Leoben, Austria

A R T I C L E I N F O

Keywords:
Direct current
Electric arc furnace
Compressibility
Magnetohydrodynamics (MHD)
Computational fluid dynamics (CFD)

A B S T R A C T

The paper reports on the behaviour and dynamics of direct current electric arc in an industrial electric arc furnace. Electric arcs are intense energy sources involved in many industrial processes. The behaviour of electric arc is simulated in a 2D axisymmetric geometry. A 40 kA current flows between two electrodes with a gap of 0.25 cm. The flow of current creates a very powerful jet up to km/s. Such speeds pose the question of the importance of compressibility and what is the extent of the effects of compressibility on arc behaviour. To assess the effect of compressibility, two different simulations are performed: an incompressible and a compressible simulation. The first simulation considers a temperature-dependent density based on experimental measurement whereas the latter adopts the ideal gas law to calculate the density variation of the plasma. The incompressible results were previously validated and compared to the well-known results predicted by the literature. The numerical results of the two models are reported and compared in terms of flow, thermal fields, and voltage drop. The results show that compressibility affects several aspects of the arc. As expected, the velocity drops when compressibility is present, however, the voltage drop increase significantly. Additionally, compressibility introduces a repetitive pattern of voltage drop over time which also depicted in the arc dynamics. The pattern is divided into three distinctive dynamics: (1) High-frequency low amplitude instabilities, followed by (2) low low-frequency high amplitude instabilities region, and finally, a relatively (3) stable interval of voltage with a bell-shaped arc.

1. Introduction

Electric arc furnace (EAF) play a crucial role in the metallurgical industry. EAF operation utilizes the heat produced by an electric arc to melt down ore and scrap materials. Over the past century, the use of EAF has experienced exponential growth, making it one of the most widely recognized applications in the metallurgical industry. The electric arc produces significant thermal energy and generates a powerful electro-vortical jet, rapidly melting the charged metal scrap/ore into liquid metal.

In general, the DC-EAF has a single electrode (cathode) mounted directly above the metal bath with adjustable height while the anode is mounted in the lower part of the crucible (furnace bottom). By applying high voltage, electrical breakdown occurs in the gap between the cathode electrode and metal scrap. The voltage breakdown results in the formation of the arc connecting the upper electrode at the cathode spot to the scrap/ore surface. The electric arc reaches temperatures exceeding 10 000 K due to Joule heating, ensuring sufficient electrical conductivity for its persistence in the gap [1]. As reported by Bowman [2], at high temperatures exceeding 10 000 k ionized atoms' velocity reach ranges of km/s, as an example the average velocity of a nitrogen atom is 3.5 km/s. Bowman [3] was able to measure the plasma velocity generated by a 2160 A DC arc, predicting a velocity of approximately 1500 m/s for a 0.07 m gap. Due to extreme conditions around the arc, experimental measurements for industrial-scale arcs are rare and hardly attempted [4,5]. Instead, numerical and mathematical models are more favourable tools to help study and understand the arcing phenomenon. Several mathematical models have been developed to predict the behaviour of high-current density jets. One of the first studies that

* Corresponding author.
E-mail address: Abdellah.kharicha@unileoben.ac.at (A. Kharicha).

https://doi.org/10.1016/j.rineng.2023.101312
Received 27 April 2023; Received in revised form 4 July 2023; Accepted 21 July 2023
Available online 22 July 2023

Nomenclature:

u	Velocity (m/s)
P	Pressure (N/m^2)
F	Lorentz Force per unit volume (N/m^3)
S	Source term per unit volume
k	Turbulence kinetic energy (m^2/s^2)
K	Thermal conductivity (W/m.K)
R	ideal gas constant (J/mol·K)
M_w	molecular weight of the gas
P_{op}	Operating Pressure(N/m^2)
T	Temperature (K)
c_p	Specific heat at constant pressure (J/kg.K)
J	Current density (A/m^2)
Rad_{loss}	Experimental radiation loss (w/m3)
B	Magnetic field (T)
c_v	Specific heat at constant volume (J/kg.K)
I_0	Applied current (A)
dV	Control volume

Greeks

ρ	Density (kg/m^3)
μ_{eff}	Effective Viscosity (N.s/m^2)
σ	Electrical conductivity (S/m)
ε	Turbulence dissipation rate (m^2/s^3)
μ_0	vacuum permeability (H/m)
γ	ratio of specific heats (c_p/c_v)
$\Delta\varphi$	Voltage drop (V)

Subscripts

z	Axial coordinates
r	Radial coordinates
θ	Azimuthal coordinates

attempted to understand the electric arc was done by Ushio et al. [6]. The study considered turbulent Naiver Stokes, energy equation, and Maxwell equations of the arc with some assumptions for current distribution. Szekely et al. [1] used a comparable model and were the first to predict the different heat transfer mechanisms from the arc to the metal bath by coupling the arc with metal bath regions. Jordan et al. [4] conducted measurements on a free-burning DC arc of 10 kA and measured several electric properties and cathode spot radius. "The paper reported a constant current density of 4.4 $\times$ 10^7 A/m^2. Bowman estimated the cathode current density as 3.5 $\times$ 10^7 A/m^2 [7]. Both estimations were in the same order of magnitude and are commonly used in high-power DC arcs with Local Thermal Equilibrium (LTE) modelling. The thermophysical and electrical properties of plasma for several gases including air were computed at high temperatures and generally adopted for high DC arc simulation [8,9]. Qian et al. [10] performed a 2D axisymmetric study for a DC high-power arc for two different current values and arc gaps. The study concluded that arc jet velocity is affected more by the applied current while the higher heat transfer to the bath area is accomplished for smaller arc gaps. Ramirez [11] developed a mathematical model specifically focused on the arc and liquid metal bath in a DC-EAF. The model utilized the potential approach to solve the electromagnetic field, the electric potential method yielded better agreement compared to the magnetic approach, particularly when compared with argon arc welding data. The study extensively explored various aspects of the arc, including cathode current density, arc jet velocity, the impact of compressibility, and the interaction with the metal bath. Decoupling the arc and metal bath was considered valid since changes in the metal bath temperature had minimal impact on the arc. The study highlighted that the key factors influencing the arc's performance were the initial arc gap and the total applied current. A significant contribution of the study was the development of dimensionless parameters for characterizing the arc, such as arc shape, magnetic flux, axial velocity, and temperature within the arc. Ramírez assessed the effect of compressibility in DC industrial arc. The study showed that considering compressibility leads to lower arc speed, temperature distribution, and voltage drop, while higher plasma density was observed. Wang et al. [12] studied the flow and heat transfer coupled with Maxwell's equation inside the arc region and the molten bath. The study concluded that convection and radiation are the main modes of heat transfer from the arc to the metal bath. Ramírez [13] studied the effect of different gases as an atmosphere for the arc and concluded that air is the most efficient gas to heat up the liquid bath. The presence of carbon oxides can improve heating efficiency. Reynolds et al. [14–16]conducted a scientific investigation in which they developed numerical models to simulate the behaviour of DC arc plasma in both 2D and 3D computational frameworks. The models encompassed the behaviour of single-phase arcs, as well as the impact of the arc on the underlying slag layer. While the model successfully predicted a transition between steady and unsteady arc behaviour, it assumed of constant arc properties with temperature. Despite this limitation, the simulation of multiphase arc impingement demonstrated reasonable agreement with experimental measurements. The voltage drop across the domain between the computational model and semi-empirical correlations extracted from experimental measurements [16]. The voltage drop in the simulation was significantly lower than the semi-empirical value, but no clear explanation for this difference was provided. Trelles [17] investigated the behaviour of a DC arc plasma torch using two temperature models in 3D. The study included the compressibility effect while neglecting the impact of turbulence. The study captured several arc aspects, including shear-flow instabilities and coherent flow structures. Guo et al. [18] examined the behaviour of a non-transferred argon-hydrogen DC arc inside a plasma torch. The findings revealed a decrease in voltage as the current increased. While the increase in flow rate increases the voltage. It should be noted, however, that the study assumed an incompressible flow, despite the predicted high velocity of 1600 m/s at the core of the jet. In their study, Murphy et al. [19] determined that the influence of compressibility becomes significant in high-velocity and turbulent plasmas, particularly when the velocity approaches sonic speeds.

From the stated literature, the influence of compressibility on the behaviour of high current density electric arcs remains largely unexplored. This study aims to investigate the dynamics of an industrial-scale electric arc, with a particular focus on addressing the impact of compressibility on flow characteristics. Using a transient 2D axisymmetric domain, the flow, thermal, and magnetohydrodynamics (MHD) fields are solved in a coupled fashion. The study aims to analyse and compare incompressible and compressible models, particularly regarding the voltage drop. By examining these models, we can gain valuable insights into the complex nature of high current density electric arcs.

To achieve these objectives, the paper is organized as follows: Section I provides the introduction and objective. Section II covers the model formulation, boundary conditions, and the equations solved. Section III presents the obtained results for both the incompressible and compressible models. Section IV provides a comprehensive discussion and analysis of the results, highlighting the observed differences. Finally, Section V presents the concluding remarks and key outcomes of the study.

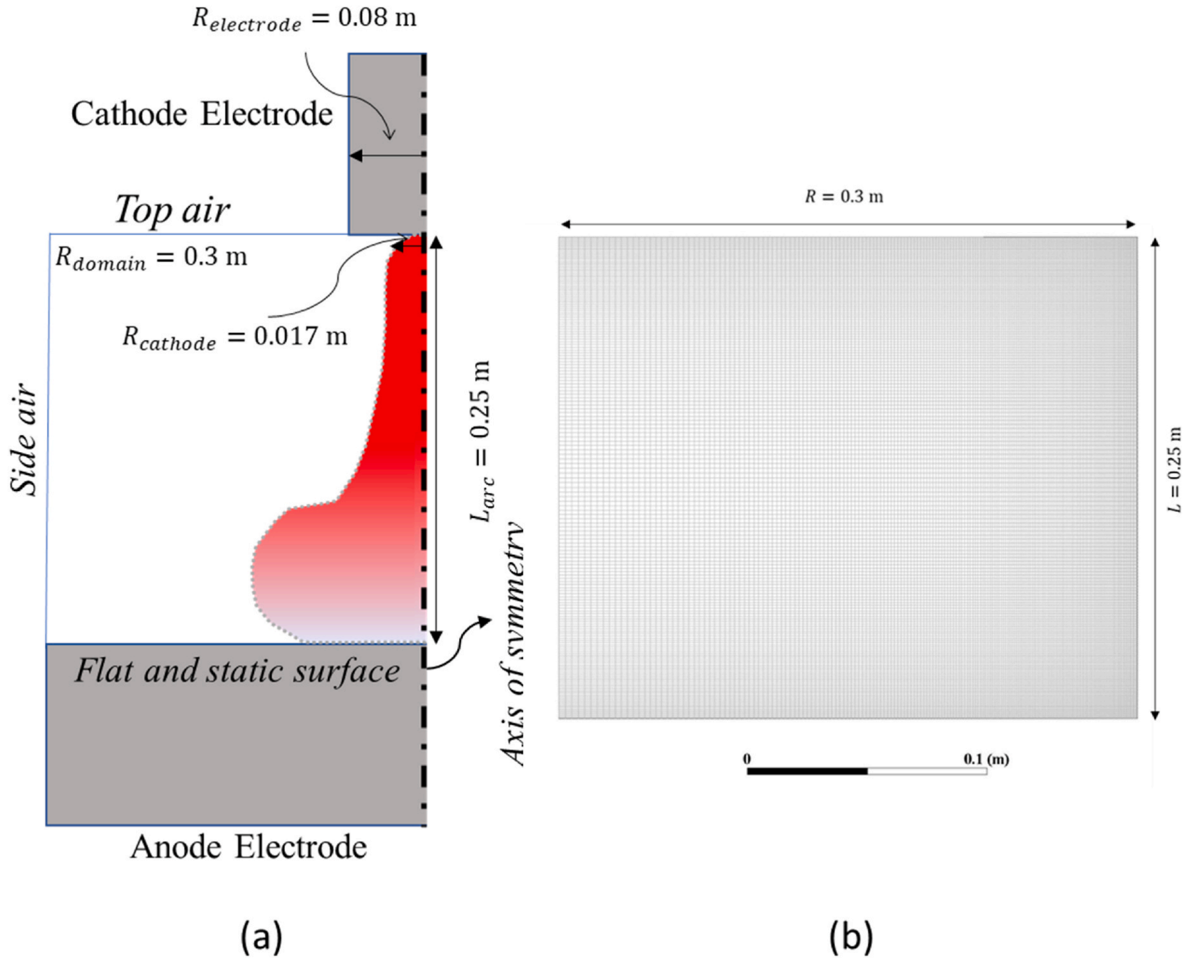

Fig. 1. (a) 2D axisymmetric Geometry of arc domain; the red part resembles the approximate arc shape. (b) Meshed domain constituted of 40 000 finite volume cells. (For interpretation of the references to colour in this figure legend, the reader is referred to the Web version of this article.)

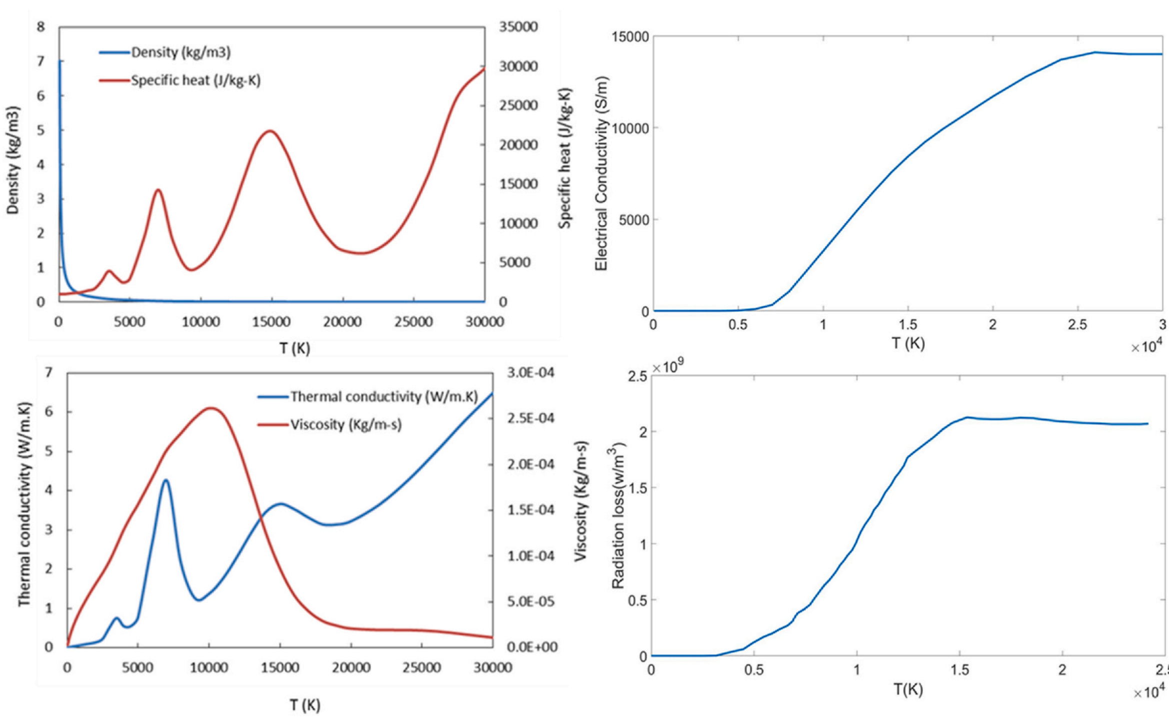

Fig. 2. Thermo-physical and electrical properties of air as functions of temperature.

Table 1
Shows the boundary conditions of the induction equation inside the domain.

Boundary	Flow	Temperature	Magnetic Field
Electrode	$u_r = u_z = 0$	$T = 4000K$	$\frac{\partial B_\theta}{\partial z} = 0$
Top air	$\frac{\partial u_r}{\partial z} = 0, u_z = 0$	$\frac{\partial T}{\partial z} = 0$	$B_\theta = \frac{I_0 \mu_0}{2\pi r}$
Side air	$u_r = u_z = 0$	$\frac{\partial T}{\partial r} = 0$	$B_\theta = \frac{I_0 \mu_0}{2\pi r}$
Flat and static surface	$u_r = u_z = 0$	$T = 1800K$	$\frac{\partial B_\theta}{\partial z} = 0$
Axis of Symmetry	$\frac{\partial u_z}{\partial r} = 0, u_r = 0$	$\frac{\partial T}{\partial r} = 0$	$B_\theta = 0$

2. Methodology

In this study, the physical configuration resembles a 2D axisymmetric model consisting of a cylindrical container filled with air in direct contact with two solid electrodes from top and bottom. The cylinder resembles the arc and its microenvironment. Fig. 1 a shows the 2D axisymmetric configuration of the domain. The cylinder has a height of 25 cm (arc gap), and a radius of 30 cm. Simulations are operated under the assumption of local thermal equilibrium (LTE) condition. LTE assumptions mean that all particles inside the system are in thermal equilibrium thus plasma can be modeled as a single phase using the thermodynamic relationships. The current flowing through the arc is 40 kA. The arc structure shown in Fig. 1 a is a schematic of an approximate bell-shaped arc structure. In reality, the arc extremities are defined according to the temperature of 10 000 K. This is based on the fact that higher than this temperature plasma conductivity is high enough to sustain electric current flow. The mesh is structured hexahedral mesh consisting of 40 000 finite volume elements Fig. 1 b.

2.1. Governing equations

The model is based on a single-phase flow's local thermal equilibrium (LTE) assumption. LTE means that the plasma properties are solely a function of temperature. This enables solving the model in the continuum regime as a single-phase compressible flow in all the domain. The model is simulated by solving the continuity, momentum, energy, and induction equations. The Induction equation is needed to account for the effects of electromagnetism and magnetohydrodynamics (MHD). Moreover, due to the high velocity, the turbulence effect is accounted for by including the standard K-epsilon (k-ε) turbulence model [20]. The numerical simulations were performed using ANSYS Fluent® software. The electromagnetic equations and the Lorentz force were computed using user-defined functions (UDF). The coupled algorithm was used to solve the pressure-velocity coupling.

Two different simulations are carried out to analyse the effect of compressibility on the arc dynamics. The first simulation relates the density in addition to thermo-physical and electrical properties to the temperature of air [21] Fig. 2. The density was measured at different temperatures up to 30 000 K, no link thus is present between pressure and the density in the incompressible model. The second simulation treats the plasma as an ideal gas. The density is calculated according to the state equation and is affected by the pressure and temperature (equation (2)). The thermo-physical and electrical properties are computed similarly to the first case based on Fig. 2. This enables us to assess the effect of compressibility without any other interference from different variables. The equations are shown below:

Continuity Equation:

$$\frac{\partial \rho}{\partial t} + \frac{1}{r}\frac{\partial(\rho r u_r)}{\partial r} + \frac{\partial(\rho u_z)}{\partial z} = 0 \quad (1)$$

Equation of state:

$$\rho = \frac{P_{op} + P}{\frac{R}{M_w} T} \quad (2)$$

Momentum Equation:

$$\begin{gathered}
\frac{\partial(\rho u_z)}{\partial t} + \frac{1}{r}\frac{\partial(\rho r u_z u_z)}{\partial z} + \frac{1}{r}\frac{\partial(\rho r u_z u_r)}{\partial r} = -\frac{\partial P}{\partial z} + \frac{1}{r}\frac{\partial}{\partial z}\left[r\mu_{reff}\left(2\frac{\partial u_z}{\partial z} - \frac{2}{3}(\nabla.\vec{u})\right)\right] \\
+\frac{1}{r}\frac{\partial}{\partial r}\left[r\mu_{reff}\left(\frac{\partial u_z}{\partial r} + \frac{\partial u_r}{\partial z}\right)\right] + F_z \\
\frac{\partial(\rho u_r)}{\partial t} + \frac{1}{r}\frac{\partial(\rho r u_z u_r)}{\partial z} + \frac{1}{r}\frac{\partial(\rho r u_r u_r)}{\partial r} = -\frac{\partial P}{\partial r} + \frac{1}{r}\frac{\partial}{\partial z}\left[r\mu_{reff}\left(2\frac{\partial u_r}{\partial z} + \frac{\partial u_z}{\partial r}\right)\right] \\
+\frac{1}{r}\frac{\partial}{\partial r}\left[r\mu_{reff}\left(2\frac{\partial u_r}{\partial r} - \frac{2}{3}(\nabla.\vec{u})\right)\right] - \mu_{reff}\frac{2u_r}{r^2} + \frac{2\mu_{reff}}{3r}(\nabla.\vec{u}) + \rho\frac{u_z^2}{r} + F_r
\end{gathered} \quad (3)$$

The additional term $F_z = J_z B_\theta; F_r = -J_z B_\theta$ represents the Lorentz force, the main driver in the momentum equation inside the arc. The Turbulence K-epsilon (k-ε) model is adopted for Turbulence [20].

Turbulence model:

$$\begin{gathered}
\frac{\partial \rho k}{\partial t} + \frac{1}{r}\frac{\partial(\rho r u_r k)}{\partial r} + \frac{\partial(\rho u_z k)}{\partial z} = \frac{\partial}{\partial z}\left(\frac{\mu_{eff}}{\sigma_k}\frac{\partial k}{\partial z}\right) + \frac{1}{r}\left(r\frac{\mu_{eff}}{\sigma_k}\frac{\partial k}{\partial r}\right) - \rho\varepsilon + S_k \\
\frac{\partial \rho\varepsilon}{\partial t} + \frac{1}{r}\frac{\partial(\rho r u_r \varepsilon)}{\partial r} + \frac{\partial(\rho u_z \varepsilon)}{\partial z} = +\frac{\partial}{\partial z}\left(\frac{\mu_{eff}}{\sigma_k}\frac{\partial \varepsilon}{\partial z}\right) + \frac{1}{r}\left(r\frac{\mu_{eff}}{\sigma_k}\frac{\partial \varepsilon}{\partial r}\right) + S_\varepsilon
\end{gathered} \quad (4)$$

Energy:

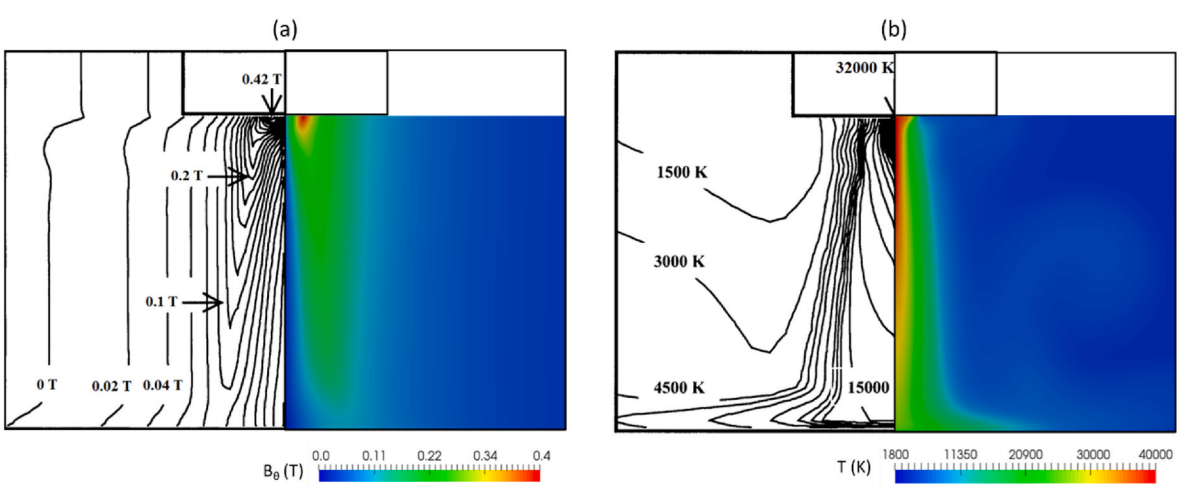

Fig. 3. Magnetic field (a) and temperature distribution (a) comparison between Alexis et al. [26] (left half) and time average over 6 ms (right half) [25].

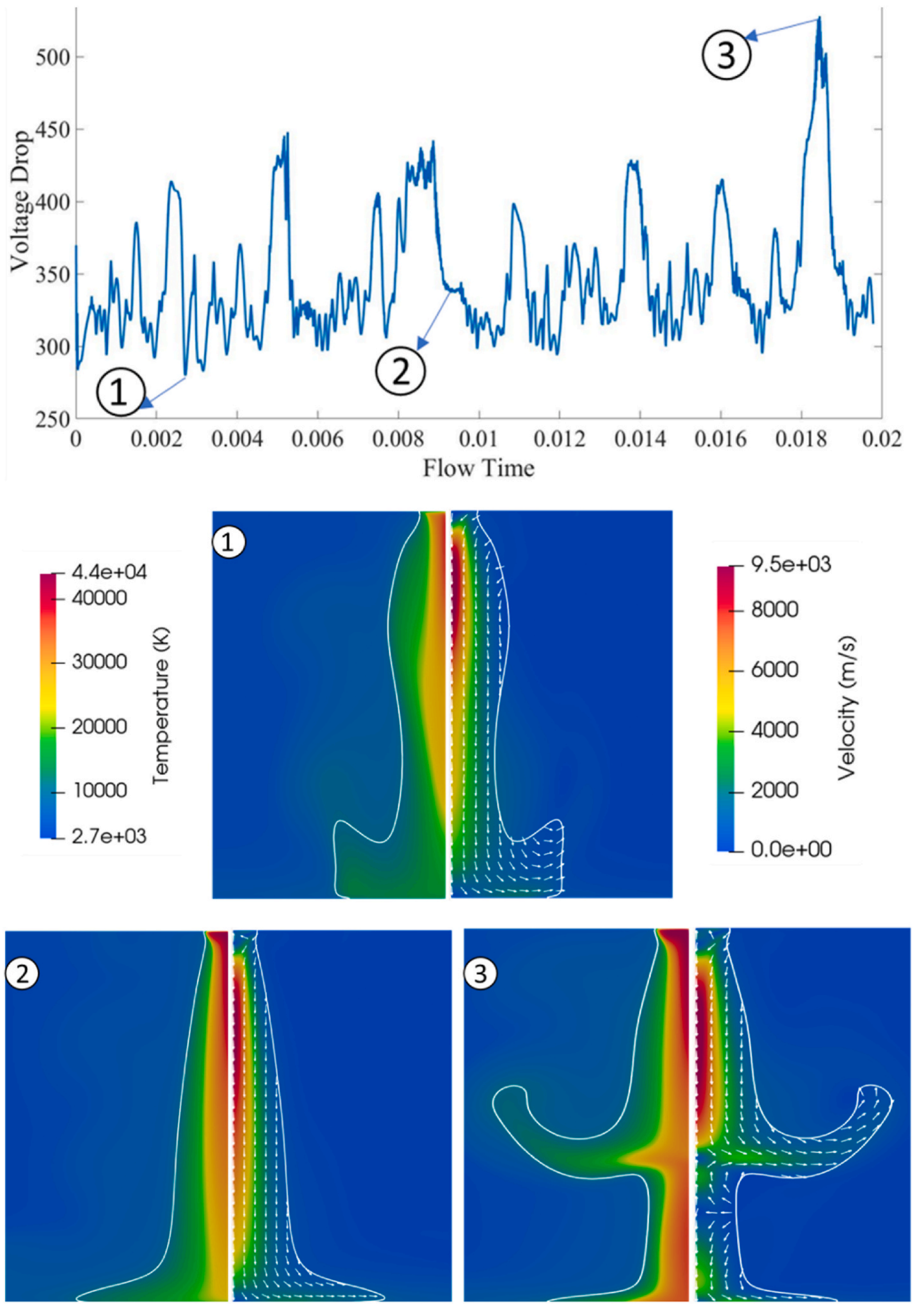

Fig. 4. Calculated voltage drop incompressible model. Points 1,2 and 3 are the minimum average and max voltage drops, respectively. The left sides show the temperature distribution and the right sides show the velocity distribution. The white contour is the isothermal line of 10 000 K.

$$\frac{\partial}{\partial t}(\rho c_p T)+\frac{1}{r}\frac{\partial(\rho r u_r c_p T)}{\partial r}+\frac{\partial(\rho u_z c_p T)}{\partial z}=\frac{1}{r}\frac{\partial}{\partial r}\left(rK_{eff}\frac{\partial T}{\partial r}\right)+\frac{\partial}{\partial z}\left(K_{eff}\frac{\partial T}{\partial z}\right)+\frac{J_z^2+J_r^2}{\sigma_e}+Rad_{loss} \tag{5}$$

Rad_{loss} is the radiation loss based on experimental measurements at atmospheric pressure [22] Fig. 2.

Induction Equation:

$$\frac{\partial B_\theta}{\partial t}+\frac{1}{r}\frac{\partial(ru_r B_\theta)}{\partial r}+\frac{\partial(u_z B_\theta)}{\partial z}=\frac{1}{r}\frac{\partial}{\partial r}\left(r\frac{1}{\sigma\mu_0}\frac{\partial B_\theta}{\partial r}\right)+\frac{\partial}{\partial z}\left(\frac{1}{\sigma\mu_0}\frac{\partial B_\theta}{\partial z}\right)+\frac{\partial}{\partial r}\left(\frac{1}{\sigma\mu_0 r}B_\theta\right) \tag{6}$$

Current density:

$$J_r=-\frac{1}{\mu_0}\frac{\partial B_\theta}{\partial z}; J_z=\frac{1}{\mu_0 r}\frac{\partial(rB_\theta)}{\partial r} \tag{7}$$

2.2. Boundary conditions

The side and top boundaries, except the cathode electrode, are set to be thermally adiabatic. The bottom of the domain has a constant temperature of 1800 K, equivalent to the liquid metal's average temperature. The temperature of the cathode spot is set to be constant and equal to 4000 K. This temperature is below the melting point of graphite and is required for high current density [23,24]. The radius of the cathode spot is calculated based on the consideration of constant current density 4.4 $\times 10^7$ A/m^2 [4] for a total current of 40 kA. The electric current flows between two solid electrodes in contact with the cylinder's horizontal

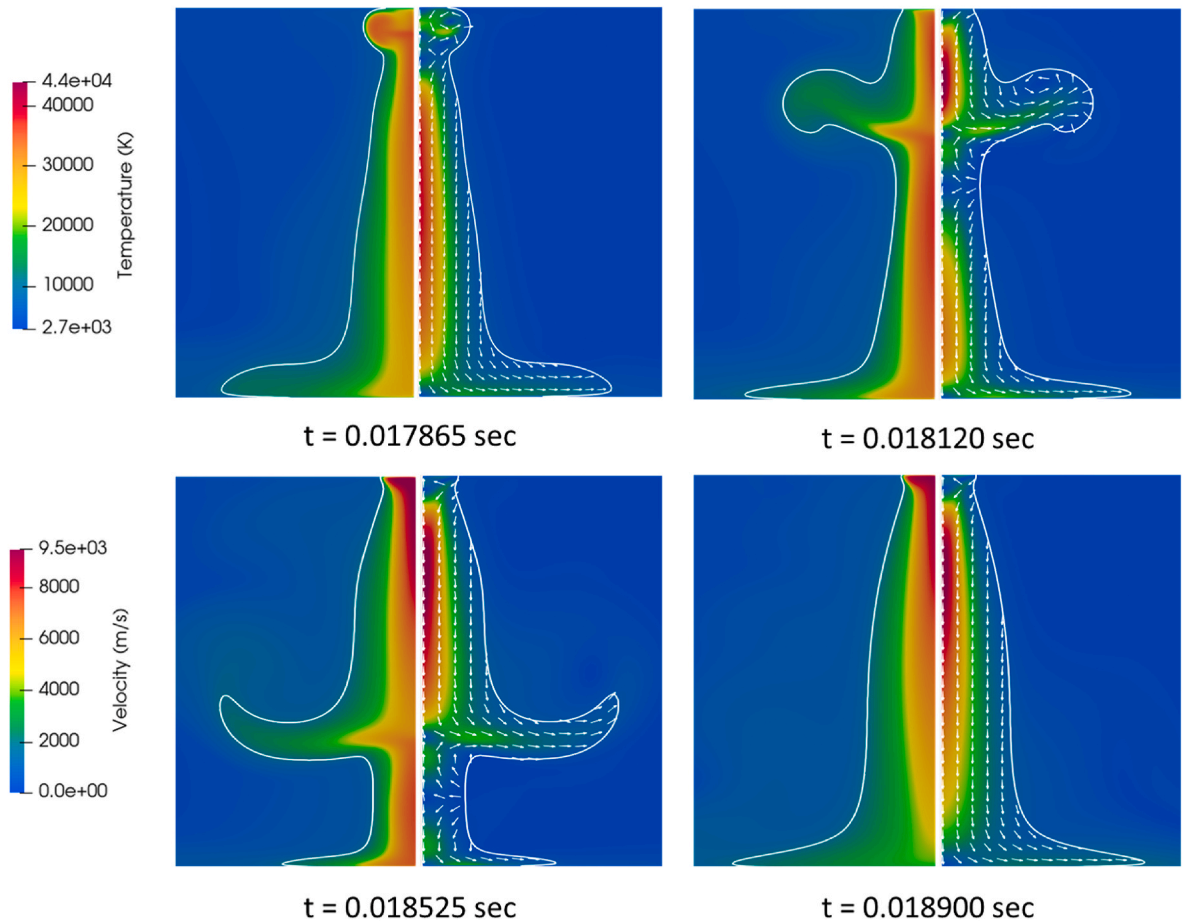

Fig. 5. Incompressible electric arc behaviour in different time snaps. The left sides show the temperature distribution and the right sides show the velocity distribution. The white contour is the isothermal line of 10 000 K.

surfaces. The cathode electrode is mounted from the top while the bottom resembles the anode surface. The lateral side of the cylinder and the top except the cathode electrode are electrically insulated. Table 1 summarizes the boundary condition of the domain. The position of the cathode spot is set to be fixed in the center of the electrode. No external magnetic field is present to interact with the applied current.

3. Results

The arc is simulated in a transient mode for a significantly long duration relative to the arc dynamics approximately 20 ms. The time step of choice is set to be very small and equal 10^{-7} s to ensure that the courant number does not exceed 1 and capture the complex behaviour of the arc. The maximum CFL = 1.9 inside the domain for incompressible while CFL = 0.7 for compressible simulation. The CFL number or (Courant-Friedrichs-Lewy) number is a dimensionless number used to ensure the stability and accuracy of solution evolving in time. Mathematically, the CFL number is defined as the product of velocity (v) and time step (Δt) divided by the grid size (Δx); CFL=(v*Δt)/Δx. For each timestep, the convergence was accomplished when absolute residuals drop below 10^{-3} for flow and 10^{-6} for the energy equation. The wall lift-off in the viscous unit (y+) was monitored in the domain. The turbulence model used was standard k-epsilon model with standard wall function. The values of (y+) ranged between 35 and 62.

The model was previously validated and compared to previous literature [25], the time average results of temperature and magnetic field were calculated for the incompressible model. The obtained results are compared with the steady state results predicted by Alexis et al. [26]. A clear similarity can be observed in Fig. 3 between the results. It is important to mention that Alexis et al. [26] used potential method, while our model utilizes the induction method.

3.1. Base case

The base case considers the flow independent of pressure and solely temperature dependent, i.e., incompressible. Fig. 4 shows different time snaps of arc thermal and velocity fields using the incompressible formulation. The white contour shown is the isothermal line of 10 000 K. Most of the current flows inside the region enclosed by this isothermal line. The electrical conductivity is high enough to enable high current density to flow when density exceeds 10 000 K. The current ingoing to the cathode from the arc region interacts with the self-induced magnetic field and induces a Lorentz force. This strong force is generated around the cathode spot, creating a strong downward jet due to symmetricity [27]. The inward radial Lorentz force acting near the cathode spot combined with very low gas density (very high temperature of the arc) results in a very high speed of up to 9500 m/s (Fig. 4). Small instabilities near the cathode spot develop at this critical speed as they travel downwards and develop gradually. The initial structure of the arc is strongly affected by these instabilities. The instabilities appear near the cathode spot and travel downwards along the arc jet [25].

The behaviour of the arc motion can be examined by analyzing the voltage drop in the arc domain as a function of time Fig. 4. The voltage drop across the domain is shown in equation (6) and is equal to the current density square J^2 divided by the electrical conductivity σ integrated over the domain and divided by the total applied current I_0.

Voltage drop:

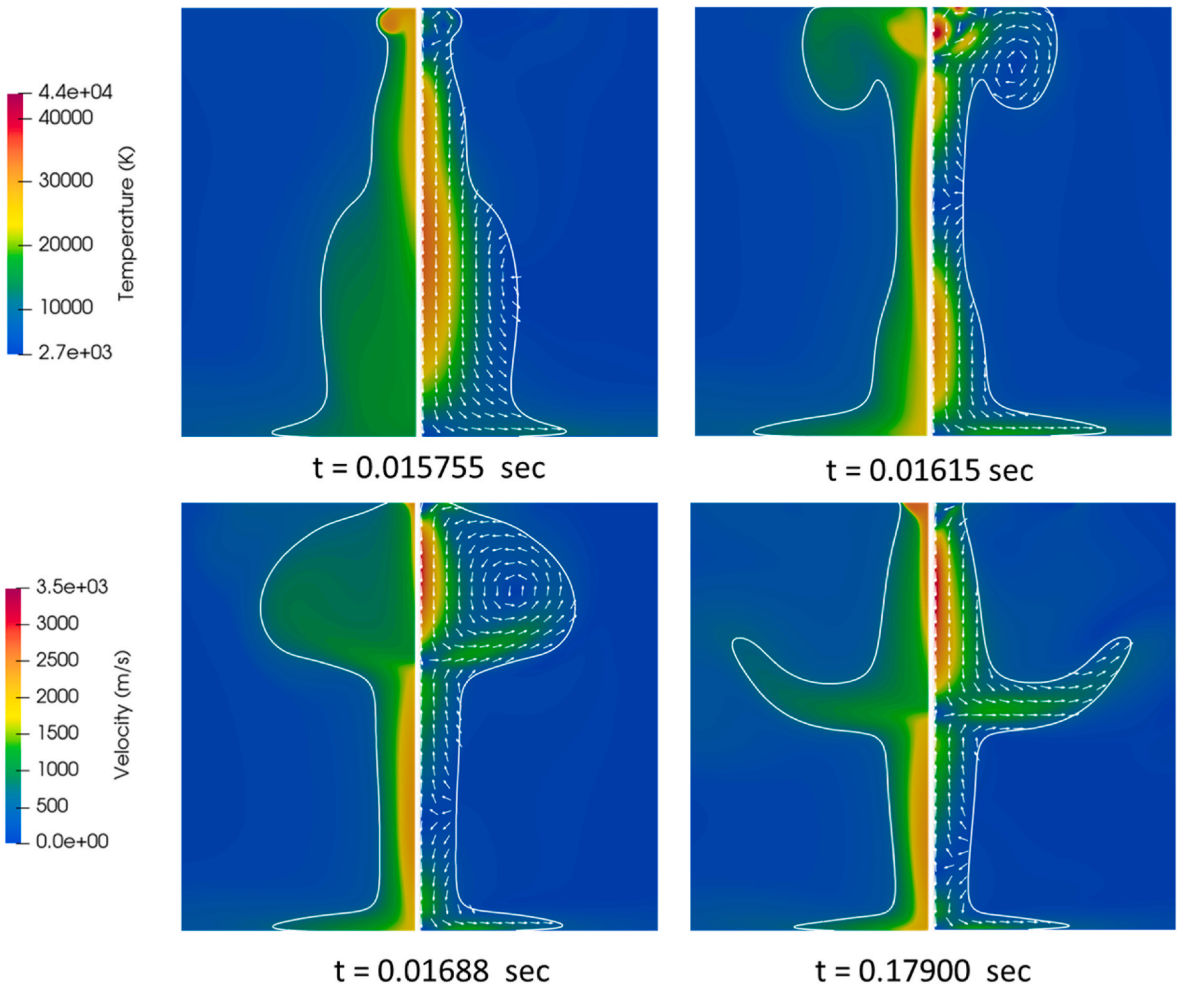

Fig. 6. Compressible electric arc behaviour using the ideal gas approach in different time snaps. The left sides show the temperature distribution and the right sides show the velocity distribution. The white contour is the isothermal line of 10 000 K.

$$\Delta\varphi = \frac{1}{I_0}\int \frac{J^2}{\sigma} dV \tag{9}$$

$\Delta\varphi$ is the voltage drop across the domain.

The shape and motion of the arc significantly affect the voltage drop. The voltage drop is maximized when the arc holds instabilities or if the arc area is spatially changing (expansion or reduction). Many peaks appear in the voltage-drop curve (Fig. 4). Sudden jumps or changes in voltage indicate the occurrence of instabilities. The graph shows that there are three distinctive structures of the arc. The first structure is when there is a local minimum of the arc voltage and occurs when the arc takes the shape of the well-known bell-shaped structure with trimmed extremities(legs) at the anode (Fig. 4 point 1). The minimum voltage observed implies that the voltage drop is minimized when the anode spot area is minimized while conserving the bell shape structure. The second structure is the full bell shape of the arc develops with flat arc legs as in Fig. 4, point 2, the voltage drop of the arc is around the average with a relatively stable arc structure. The third important feature is when the instabilities created at the cathode spot grow as they travel downwards and create hydrodynamic vortex instabilities (Fig. 4, point 3) [2,25]. At this stage, the arc has a local maximum voltage drop. The behaviour of the arc is relatively chaotic with frequency oscillation between 50 Hz and 40 kHz, and the voltage drop as a function of time appears to be random without any global outline. The average voltage drop in the arc over the simulation run time (20 ms) was equal to 340 V.

In the second simulation, the gas density was treated in a compressible ideal gas formulation. All the other thermophysical properties were computed similarly to the first simulation. Having density as the only variable enables assessing compressibility's effect without external factors. Fig. 6 shows different time snapshots of arc thermal and velocity fields for the compressible simulation. Similarly, the white contour shown is an isothermal line of 10 000 K. The first apparent effect of compressibility was the reduction in velocity magnitude from around 9500 m/s to about 3500 m/s. However, the general geometric structure of the arc is similar to the incompressible model. When examining the dynamics and behaviour of the arc, the dynamics are slower in time compared to the incompressible case in Figs. 5 and 6. For the compressible model, in Fig. 6, at time t = 0.015755 s, a small instability is generated near the cathode spot. In contrast to the observations in the incompressible simulation, the instability is not directly drifted downwards. The instability expands and grows in space without translating downwards, as shown at t = 0.01615 s. Only after significant expansion, the vortex starts to move slowly downward. The vortex needed 2.145 ms to reach half the domain, whereas in the incompressible case, it only needed 0.66 ms (approx. three times slower Fig. 5).

The voltage drop as a function of time for the compressible model is shown in Fig. 7. The arc structures closely resemble those in the incompressible arc, but some significant differences can be easily pointed out. The average voltage drop significantly increases to 445 V (105 V higher than in the incompressible arc simulation). The observed voltage is very close to what has been measured in an industrial-scale furnace of 40 kA (450 V) [5]. This is around a 1% difference. A repetitive pattern appears in the behaviour of the voltage drop as a function of time. Initially, very small but fast fluctuations of voltage instabilities

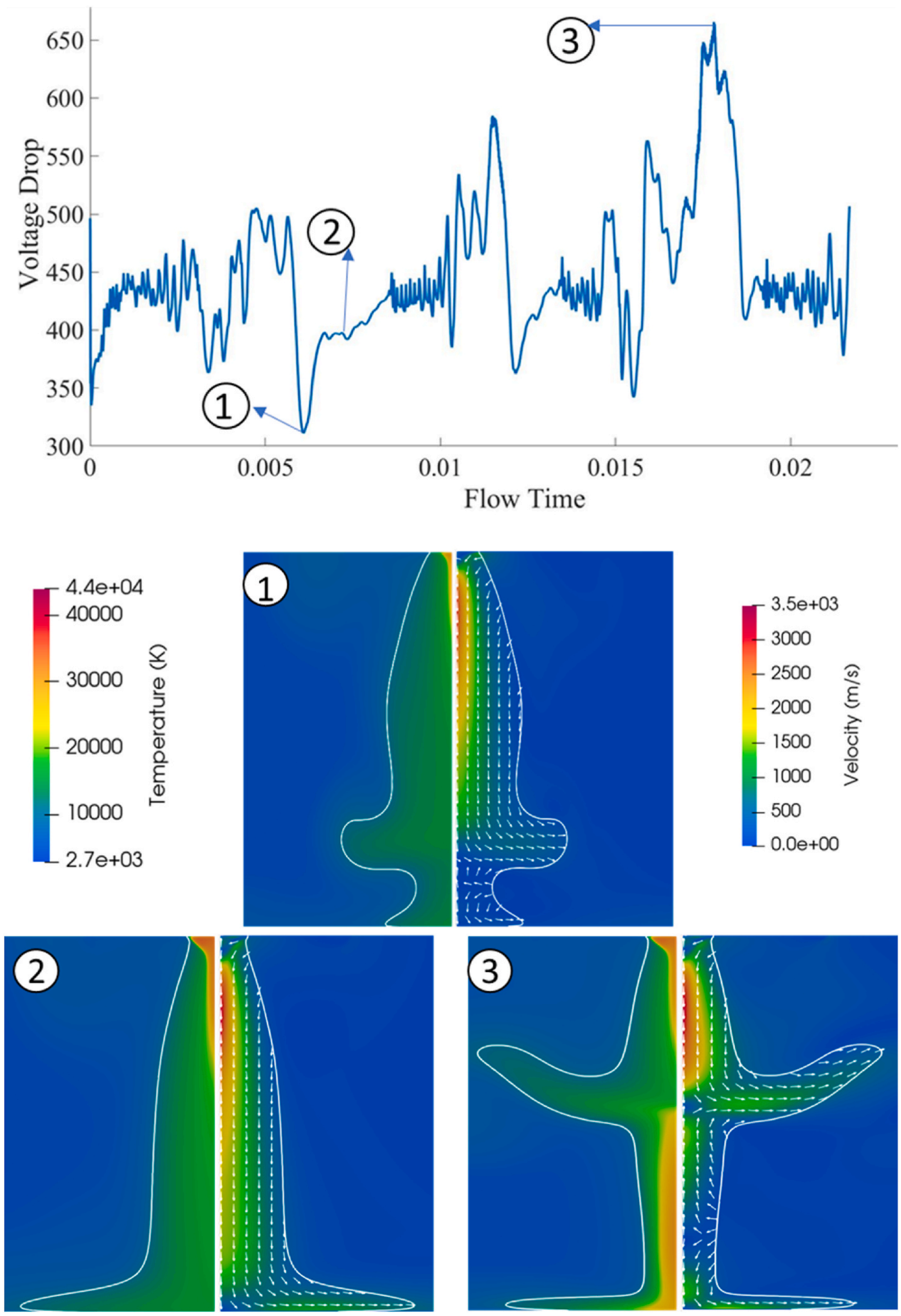

Fig. 7. Calculated voltage drop compressible model. Points 1,2 and 3 are the minimum average and max voltage drops, respectively. In the arc structure, the left sides show the temperature distribution and the right sides show the velocity distribution. The white contour is the isothermal line of 10 000 K.

occur (Fig. 8 **a**), followed by more significant amplitude fluctuations but with lower frequency (Fig. 8 **b**). The fluctuations seem to have an inversely proportional relationship between their frequency and amplitude. The small amplitude fluctuations oscillate at a high frequency of 10–20 kHz (Fig. 8a). The large amplitude fluctuations have a frequency of 1–2 kHz (Fig. 8b). This is followed by a relatively stable region as shown in Fig. 8.2 c. This pattern is periodic and is repeated three times during the simulation time of 20 ms.

Fig. 9 shows the Mach number distribution for the arc with a bell shape in both models. The Mach number $= \frac{V}{C}$ where V is the velocity and C is the speed of sound $C = \sqrt{\gamma RT}$ Υ is the ratio of specific heats (c_p/c_v) while R is the gas law constant and T is temperature. The Mach number inside the incompressible model equals 3, significantly larger than 0.3. When the Mach number exceeds 0.3, the flow is considered compressible. Compressibility should be taken into account. to prevent unphysical speeds inside the domain. The Mach number in the compressible model equals to 1.1. The effect of compressibility is apparent and shows the importance of compressibility to predict arc speeds accurately.

4. Discussion

The study shows a noticeable change in the behaviour and dynamics of the arc upon applying compressibility in plasma modelling. Compressibility cannot be neglected as it alters many critical features inside the arc. The most important changes are jet velocity magnitude, instability nature and frequency, and voltage drop. The voltage drop is a crucial factor as it is very important to accurately estimate the electric

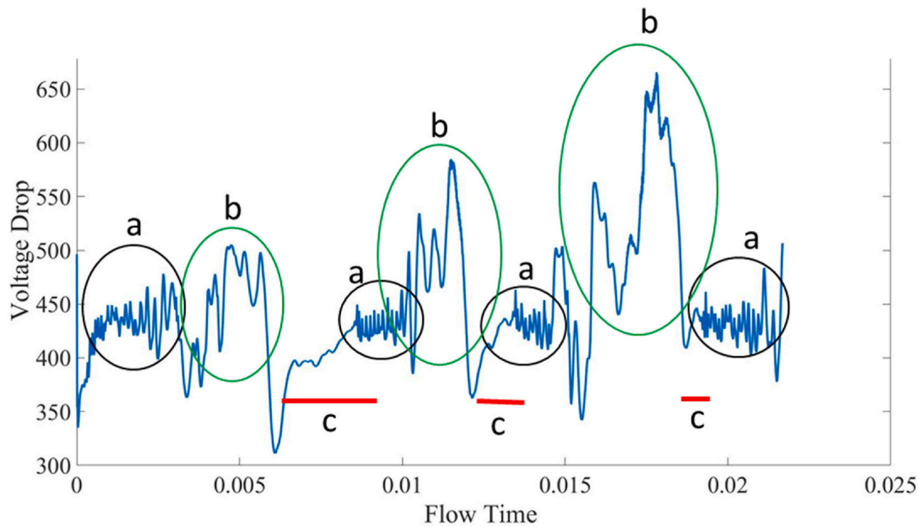

Fig. 8. Calculated voltage drop in the compressible model. (a) is high frequency and low amplitude interval, (b) low frequency and high amplitude interval, and (c) arc stable interval.

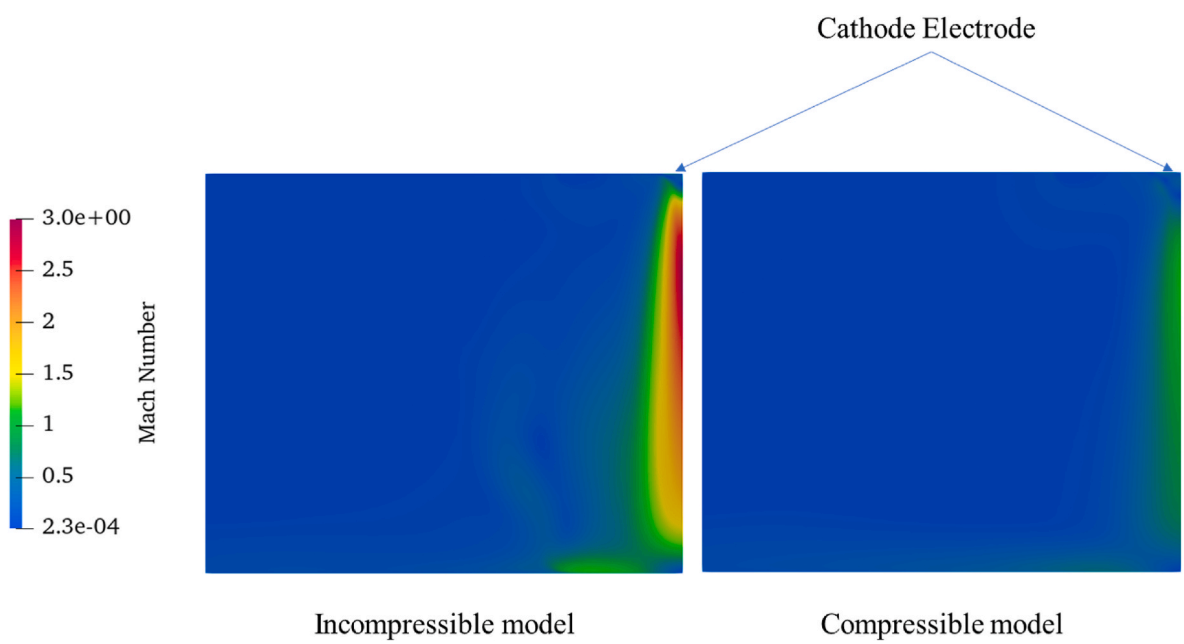

Fig. 9. Mach number comparison in incompressible and compressible model.

furnace's active power, efficiency, and operation conditions. Proper voltage drop estimation can help validate the numerical results with experimental measurements in the future without getting exposed to harsh conditions inside the furnace. Ramírez [11] studied the effect of compressibility on the arc for similar boundary conditions 40 kA and 25 cm gap. He concluded that compressibility is very important to be considered in arc simulation however, further analyses were disregarded due to significant difficulties in convergence. The study predicts that compressibility leads to lower arc velocity, increased plasma density, and decreased temperature distribution. The main difference with the current study is the prediction of lower voltage for compressible formulation without any further explanation. Reynolds [16] also noticed the voltage difference when comparing incompressible simulation with semi-empirical data obtained from measurements. He developed a computational model to study the arc-slag interaction in a DC furnace. Even though the trends were captured in the incompressible model, he noticed that the model predicted much lower voltage than the experiment.

It is important to analyse what physical difference the compressibility introduces compared to the incompressible model to understand this difference in voltage drop. Identical thermal and flow conditions were imposed for both cases incompressible and compressible. The density values of both models are displayed in Fig. 10. The same temperature field leads to different density distributions inside the computational domain. The compressible formulation leads to a higher density than the temperature-dependent (incompressible) model.

In both compressible and compressible models the specific heat is computed similarly based on temperature, so the change in density prediction will affect the system's thermal inertia. In other words, the compressible model predicts higher density. The plasma temperature will thus be lower for the compressible model compared to the incompressible model. This is observed even though the same global current is applied (40 kA). Fig. 11 shows the temperature distribution of the previously described structures in both incompressible and compressible

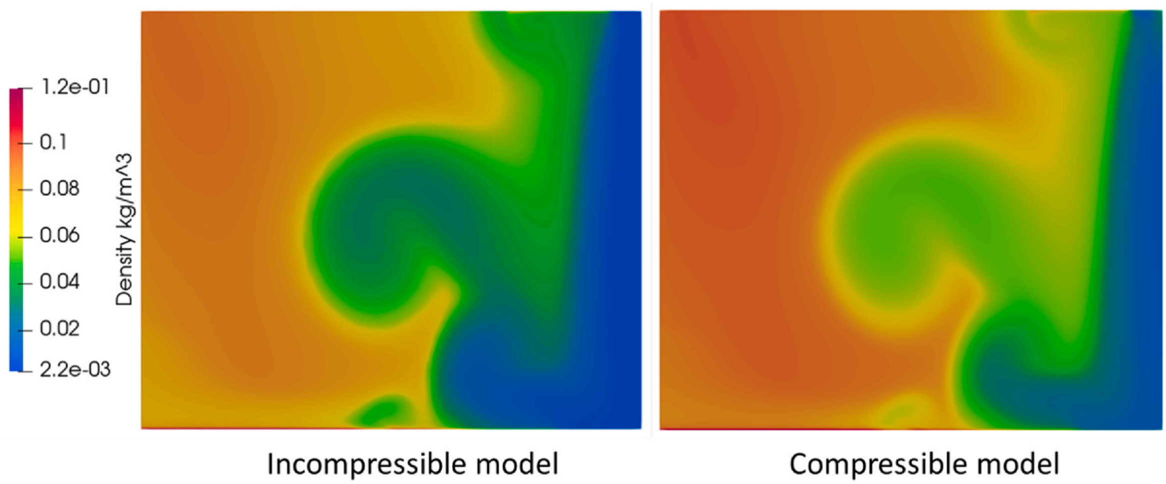

Fig. 10. Comparison between density distribution inside the domain for both models.

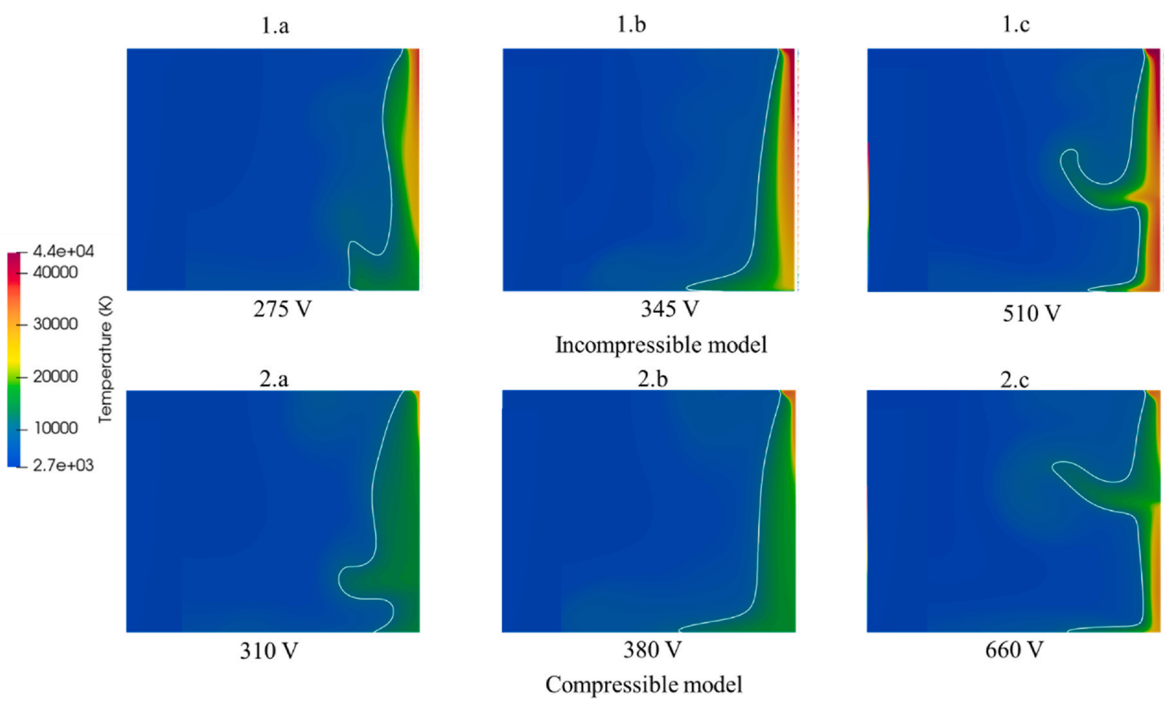

Fig. 11. Temperature distribution and voltage drop for different arc structures for both compressible and incompressible model.

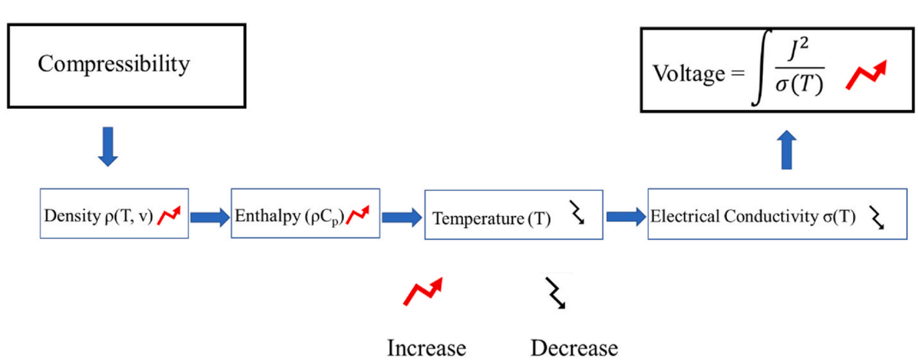

Fig. 12. Schematic diagram explaining the relation between compressibility and voltage drop.

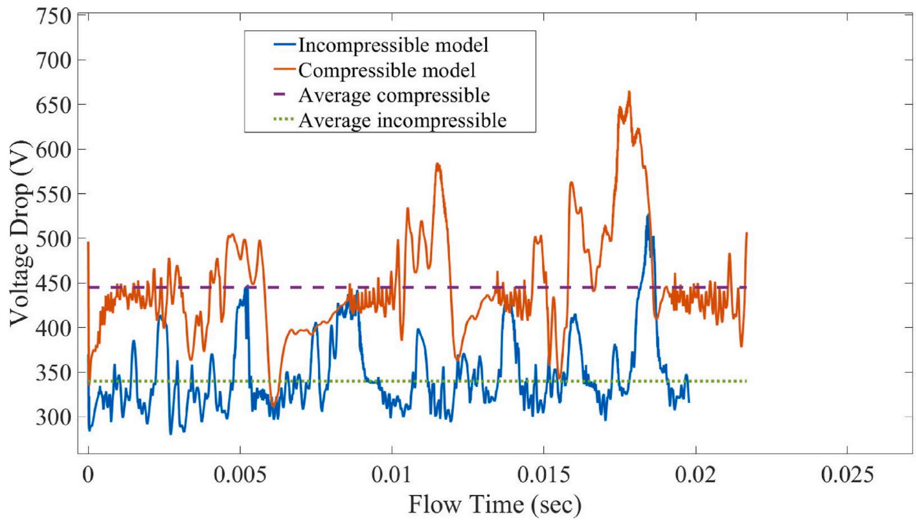

Fig. 13. Voltage drop as a function of time.

models (Figs. 4 and 7). Comparing similar structures shows that the temperature field for incompressible plasma is always higher. Additionally, the lower voltage drop is always present in the incompressible model independent of the arc structure.

A lower temperature distribution results in lower electrical conductivity distribution. Fig. 2 shows the variation of electrical conductivity with temperature. The electrical conductivity of the plasma depends solely on temperature. The voltage drop in the system is calculated according to equation (9). The electrical conductivity is inversely proportional to the voltage drop which explains the higher voltage drop in the compressible flow. Fig. 12 shows a schematic diagram illustrating how compressibility impacts the voltage drop.

The proper estimation of voltage drop is crucial to understand the electric arc behaviour during the operation of a furnace. The higher voltage predicted by the compressible model for the same current leads to a better understanding of several aspects of EAF. The power efficiency in EAF is directly affected by the voltage drop. A proper estimation of voltage drop is critical to estimate accurately the power consumption inside a furnace and evaluate the efficiency of the process. Moreover, to avoid any undesired stresses on the electric circuit and components inside the furnace the correct voltage range should be properly known before installation. The influence of compressibility extends beyond the voltage value, but also the frequency of voltage and its influence on the arc behaviour. High frequency of voltage drop can lead to undesirable interaction between the arc and furnace circuit and in some extremes leads to flickering effect [28]. This can result in unstable operation and undesirable effects such as poor power quality and reduced productivity.

The arc dynamics are also substantially influenced by the voltage variation. The high-frequency voltage interval observed in Fig. 8 a indicates very rapid instabilities. While Fig. 8 b shows instabilities that have lower frequencies but larger impact on arc structure. The faster instabilities can affect the electrical circuit more substantially while the lower frequency is linked to hydrodynamic instabilities of the arc. The compressibility also affects the arc flow dynamics. The velocity of the arc was predicted to drop by one-third of the incompressible model. Furthermore, the average temperature distribution is lower in compressible arc, however, this does not implicate that we expect the arc hydrodynamic effect and thermal effect to be less effective than what is predicted by the incompressible model. The decrease in velocity and temperature is coupled with higher density. The momentum and thermal inertia are conserved. This was previously shown when considering the different densities of plasma for same current [29]. The impingement depth remained the same for different plasma densities when the applied current was constant.

A direct comparison of the voltage drop between compressible and incompressible formulations for the arc modelling is shown in Fig. 13. The figure indicates higher voltage when adopting compressibility in simulation. The voltage calculated in an operating electric arc furnace with 40 kA was equal to 450 V by Jones et al. [5]. The average voltage predicted by our compressible model is 445 V which is around 1% difference which is a good agreement.

5. Conclusion

In conclusion, the numerical investigation presented in this study focused on analyzing the influence of compressibility on industrial electric arcs. The 2D axisymmetric induction-based model simulated the electric arc under atmospheric pressure conditions and 40 kA current for a 25 cm arc gap. By comparing the compressible and incompressible models, valuable insights were gained.

The finding of the study demonstrates several impacts of compressibility on the electrical properties of the arc. Specifically, compressibility results in higher voltage drop across the arc compared to the incompressible model. Moreover, higher voltage frequencies and a repetitive pattern in voltage were observed in the compressible model.

Furthermore, the inclusion of compressibility leads to a substantial reduction in the jet velocity of the arc approximately one-third lower than the incompressible model prediction. Additionally, lower temperature distribution and higher density within the arc are caused by compressibility.

These findings provide a possible explanation for the voltage discrepancy observed between computational models and measured data, contributing to more accurate predictions of voltage drop within the electric arc. Further improvements of the model can be to consider non-equilibrium conditions and variable cathode spot size.

Declaration of competing interest

The authors declare that they have no known competing financial interests or personal relationships that could have appeared to influence the work reported in this paper.

Data availability

The data that has been used is confidential.

Acknowledgments

The authors acknowledge financial support from the Austrian Federal Ministry of Economy, Family and Youth and the National Foundation for Research, Technology, and Development within the framework of the Christian-Doppler Laboratory for Metallurgical Applications of Magnetohydrodynamics.

References

[1] J. Szekely, J. McKelliget, M. Choudhary, Heat-transfer fluid flow and bath circulation in electric-arc furnaces and Dc plasma furnaces, Ironmak. Steelmak. 10 (1983) 169–179.

[2] B. Bowman, K. Krüger, Arc Furnace Physics, Verlag Stahleisen, Düsseldorf, 2009.

[3] B. Bowman, Measurements of plasma velocity distributions in free-burning DC arcs up to 2160 a, J. Phys. D Appl. Phys. 5 (1972) 1422–1432, https://doi.org/10.1088/0022-3727/5/8/309.

[4] G.R. Jordan, B. Bowman, D. Wakelam, Electrical and photographic measurements of high-power arcs, J. Phys. D Appl. Phys. 3 (1970) 1089–1099, https://doi.org/10.1088/0022-3727/3/7/313.

[5] R.T. Jones, Q.G. Reynolds, M.J. Alport, DC arc photography and modelling, Miner. Eng. 15 (2002) 985–991, https://doi.org/10.1016/S0892-6875(02)00167-X.

[6] M. Ushio, F. Matsuda, Mathematical modelling of flow field and heat transfer of welding arc, Int. Symp. Japan Weld. Soc. 1 (1982) 49–54.

[7] B. Bowman, Properties of arcs in DC furnaces, in: 1994 Electr. Furn. Conf. Proc., 1994, pp. 111–120.

[8] P. Fauchais, A. Vardelle, Thermal Plasmas, Springer Science & Business Media, 1997, https://doi.org/10.1109/27.650901.

[9] A.B. Murphy, Transport coefficients of air, argon-air, nitrogen-air, and oxygen-air plasmas, Plasma Chem. Plasma Process. 15 (1995) 279–307, https://doi.org/10.1007/BF01459700.

[10] F. Qian, B. Farouk, R. Mutharasan, Modeling of fluid flow and heat transfer in the plasma region of the dc electric arc furnace, Metall. Mater. Trans. B 26 (1995) 1057–1067, https://doi.org/10.1007/BF02654108.

[11] M.A. Ramírez-argáez, Mathematical Modeling of DC Electric Arc Furnace Operations, 2003.

[12] F. Wang, Z. Jin, Z. Zhu, Numerical study of dc arc plasma and molten bath in dc electric arc furnace, Ironmak. Steelmak. 33 (2006) 39–44, https://doi.org/10.1179/174328105X71326.

[13] M.A. Ramírez-Argáez, C. González-Rivera, G. Trápaga, Mathematical modeling of high intensity electric arcs burning in different atmospheres, ISIJ Int. 49 (2009) 796–803, https://doi.org/10.2355/isijinternational.49.796.

[14] Q.G. Reynolds, R.T. Jones, B.D. Reddy, Mathematical and computational modelling of the dynamic behaviour of direct current plasma arcs, Proc. 12th Int. Ferroalloys Congr. Sustain. Futur. 110 (2010) 789–801.

[15] Q.G. Reynolds, Computational modelling of shear-layer instabilities and vortex formation in DC plasma arcs, Miner. Eng. 63 (2014) 35–44, https://doi.org/10.1016/j.mineng.2013.10.027.

[16] Q.G. Reynolds, Computational modeling of arc–slag interaction in DC furnaces, Jom 69 (2017) 351–357, https://doi.org/10.1007/s11837-016-2166-9.

[17] J.P. Trelles, Computational study of flow dynamics from a dc arc plasma jet, J. Phys. D Appl. Phys. 46 (2013), https://doi.org/10.1088/0022-3727/46/25/255201.

[18] Z. Guo, S. Yin, H. Liao, S. Gu, Three-dimensional simulation of an argon-hydrogen DC non-transferred arc plasma torch, Int. J. Heat Mass Tran. 80 (2015) 644–652, https://doi.org/10.1016/j.ijheatmasstransfer.2014.09.059.

[19] A.B. Murphy, D. Uhrlandt, Foundations of high-pressure thermal plasmas, Plasma Sources Sci. Technol. 27 (2018), 063001, https://doi.org/10.1088/1361-6595/aabdce.

[20] T.-H. Shih, W.W. Liou, A. Shabbir, Z. Yang, J. Zhu, A new k-ε eddy viscosity model for high Reynolds number turbulent flows, Comput. Fluids 24 (1995) 227–238.

[21] M.I. Boulos, P. Fauchais, E. Pfender, Thermal Plasmas, Springer Science & Business Media, 1994.

[22] J.C. Morris, G.R. Bach, R.U. Krey, R.W. Liebermann, J.M. Yos, Continuum radiated power for high-temperature air and its components, AIAA J. 4 (1966) 1223–1226, https://doi.org/10.2514/3.3652.

[23] J. McKelliget, J. Szekely, The modelling of fluid flow and heat transfer in arc furnaces, in: 5th Arc Furn. Meet., 1985.

[24] J. Haidar, A.J.D. Farmer, Surface temperature measurements for tungsten-based cathodes of high-current free-burning arcs, J. Phys. D Appl. Phys. 28 (1995) 2089–2094, https://doi.org/10.1088/0022-3727/28/10/014.

[25] H. Barati, A. Kharicha, M. Al-Nasser, D. Kreuzer, G. Hackl, M. Gruber, A. Ishmurzin, C. Redl, I.O. Teplyakov, M. Wu, A. Ludwig, MHD instability at the cathode spot as the origin of the vortex formation in high-intensity plasma arcs, J. Phys. Commun. 6 (2022), https://doi.org/10.1088/2399-6528/ac4b49.

[26] J. Alexis, M. Ramirez, G. Trapaga, P. Jönsson, Modeling of a DC Electric Arc Furnace—Heat Transfer from the Arc, vol. 40, 2000, pp. 1089–1097.

[27] A. Kharicha, M. Al-Nasser, H. Barati, E. Karimi-Sibaki, A. Vakhrushev, M. Abdi, A. Ludwig, M. Wu, Tornados and cyclones driven by Magneto-hydrodynamic forces, Eur. J. Mech. B Fluid 94 (2022) 90–105, https://doi.org/10.1016/j.euromechflu.2022.02.001.

[28] R.T. Jones, Q.G. Reynolds, T.R. Curr, D. Sager, Some myths about DC arc furnaces, J. South. African Inst. Min. Metall. 111 (2011) 665–673.

[29] M. Al-Nasser, A. Kharicha, H. Barati, C. Pichler, G. Hackl, M. Gruber, A. Ishmurzin, C. Redl, M. Wu, A. Ludwig, Toward a simplified Arc Impingement model in a direct-current electric arc furnace, Metals 11 (2021) 1482.